Computers and Structures 288 (2023) 107157

Contents lists available at ScienceDirect

Computers and Structures

journal homepage: www.elsevier.com/locate/compstruc

Neural networks for fatigue crack propagation predictions in real-time under uncertainty

V. Giannella [a,*], F. Bardozzo [b], A. Postiglione [b], R. Tagliaferri [b], R. Sepe [a], E. Armentani [c]

[a] Department of Industrial Engineering, University of Salerno, via Giovanni Paolo II, 132, Fisciano, SA, Italy
[b] Department of Management and Innovation Systems, University of Salerno, Via Giovanni Paolo II, 132, Fisciano, SA, Italy
[c] Department of Chemical, Materials and Production Engineering, University of Naples "Federico II", Piazzale V. Tecchio, 80, 80125 Napoli, Italy

ARTICLE INFO

Keywords:
Computational mechanics
Crack propagation
Neural networks
Uncertainty
Life prediction
Structural health monitoring

ABSTRACT

Crack propagation analyses are fundamental for all mechanical structures for which safety must be guaranteed, e.g. as for the aviation and aerospace fields. The estimation of life for structures in presence of defects is a process inevitably affected by numerous and unavoidable uncertainty and variability sources, whose effects need to be quantified to avoid unexpected failures or excessive conservativism.

In this work, residual fatigue life prediction models have been created through neural networks for the purpose of performing probabilistic life predictions of damaged structures in real-time and under stochastically varying input parameters. In detail, five different neural network architectures have been compared in terms of accuracy, computational runtimes and minimum number of samples needed for training, so to determine the ideal architecture with the strongest generalization power. The networks have been trained, validated and tested by using the fatigue life predictions computed by means of simulations developed with FEM and Monte Carlo methods. A real-world case study has been presented to show how the proposed approach can deliver accurate life predictions even when input data are uncertain and highly variable.

Results demonstrated that the "H1-L1" neural network has been the best model, achieving an accuracy (Mean Square Error) of 4.8e-7 on the test dataset, and the best and the most stable results when decreasing the amount of data. Additionally, since requiring only very few parameters, its potential applicability for Structural Health Monitoring purposes in small cost-effective GPU devices resulted to be attractive.

1. Introduction

Mechanical components generally fail at notches or at some critical locations due to microscopic deformations or defects from which cracks nucleate [1–3]. Although the material processing technologies have been greatly improved in the last years, it is still practically impossible to manufacture components without any defect [4]. Holes, voids or cracks are commonly found in components after almost any manufacturing process, from traditional processes (e.g. welding [5–9]), to composite manufacturing [10] and especially for the latest additive manufacturing technologies [11,12]. Predicting the residual fatigue life of structures has become an essential issue in numerous engineering sectors in order to prevent safety accidents and economic losses [13,14].

The crack nucleation process is usually followed by Fatigue Crack-Growth (FCG) through the section/thickness of components that can consequently lead to the complete failure of a structure. Unfortunately, FCG processes show considerable variability even in "identical" repeated laboratory tests, e.g. see [15]. This variability is due to geometrical factors, material scattering, statistical uncertainty, approximations, errors and to all those factors that can influence the structural integrity of a component during its service life [16–19]. Quantifying and controlling all these factors is essential to enhance the competitiveness in designing fatigue-safe products, although measuring their impact on the predictions can be rather demanding, e.g. because the distributions of parameters are generally unknown and the related experimental measurements are either impractical (e.g. due to unacceptable time/cost) or even impossible in many cases. Therefore, the need to resort to advanced tools for predicting the life of structures, possibly that monitor the structures and update their predictions in real-time, appears to be essential.

With the unprecedented and massive development of computer science, various numerical simulation techniques have been developed to estimate the life of mechanical structures [20–22], so to increase safety

* Corresponding author.
E-mail address: vgiannella@unisa.it (V. Giannella).

https://doi.org/10.1016/j.compstruc.2023.107157
Received 3 March 2023; Accepted 27 August 2023
Available online 2 September 2023
0045-7949/© 2023 The Author(s). Published by Elsevier Ltd. This is an open access article under the CC BY-NC-ND license (http://creativecommons.org/licenses/by-nc-nd/4.0/).

Nomenclature

a	crack length
A_{nom}	nominal (uncracked) cross section of plate
a_μ	mean value for crack length
a_σ	standard deviation for crack length
C	coefficient of Paris' law
da/dN	crack-growth rate
P	Applied load amplitude
P_μ	mean value for the applied load amplitude
P_σ	standard deviation for the applied load amplitude
f_l	Number of filters per convolutional layer
f	Newman's crack closure coefficient
m	exponent of Paris' law
N_f	residual fatigue life, reference value
$N_f{}^*$	residual fatigue life, NN prediction
n_l	number of neurons per dense layer
K	stress intensity factor
K_I	Mode-I stress intensity factor
K_{max}	maximum value of stress intensity factor
K_{min}	minimum value of stress intensity factor
R	load ratio $= K_{min}/K_{max}$
R^2	Coefficient of determination
s	number of samples
s_{max}	applied maximum stress
t	specimen thickness
t_μ	mean value for specimen thickness
t_σ	standard deviation for specimen thickness
α	constraint factor
ΔK	range of stress intensity factor
μ	mean value
σ	standard deviation
σ_{nom}	nominal (uncracked) stress value
σ_I	Maximum principal stress value
σ_{UTS}	ultimate tensile strength
σ_{ys}	yield stress
σ_0	flow stress
ADAM	Adaptive Model Estimation
CGR	Crack-Growth Rate
FCG	Fatigue Crack-Growth
FEM	Finite Element Method
GPU	Graphics Processing Unit
LM	Levenberg-Marquardt
MAE	Mean Average Error
MC	Monte Carlo
MSE	Mean Squared Error
NN	Neural Network
RMS	Root Mean Square
SGD	Stochastic Gradient Descent
SHM	Structural Health Monitoring

and/or to reduce maintenance costs (e.g. by enlarging inspection intervals). Such improvements have been accomplished by also leveraging on the "damage tolerance" designing philosophy that allowed to better understand and control the damaging process of structures. Nowadays, crack propagation processes are numerically simulated by means of several methodologies (such as boundary element method [23–28], meshless method [29,30], Finite Element Method (FEM) [31–34], etc.) allowing to find new insights and knowledge about the evolution of defects in many types of materials and structures. Among these methods, FEM represents the most widely recognized method thanks to its generality, robustness and widespread employment in industry. Currently, FEM allows to solve fracture problems with high accuracy in reasonable

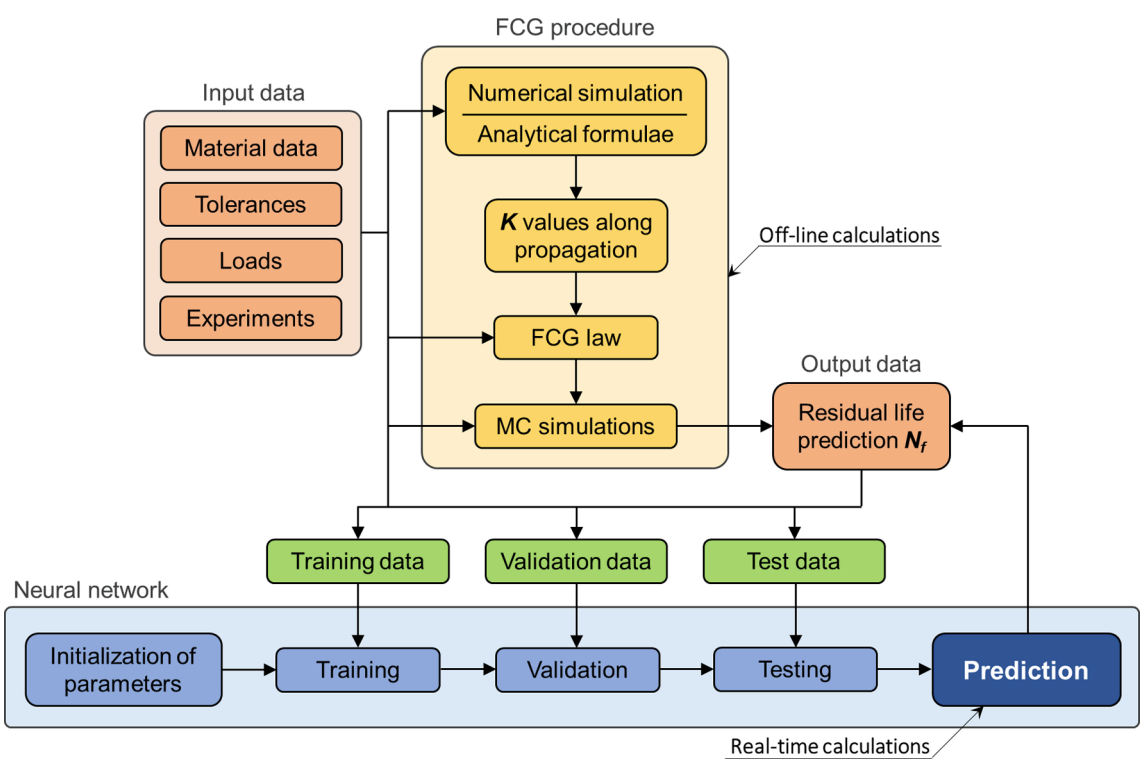

Fig. 1. Overall description of the approach for fatigue crack-growth assessments under uncertainty using FEM, Monte Carlo simulations and Neural Networks.

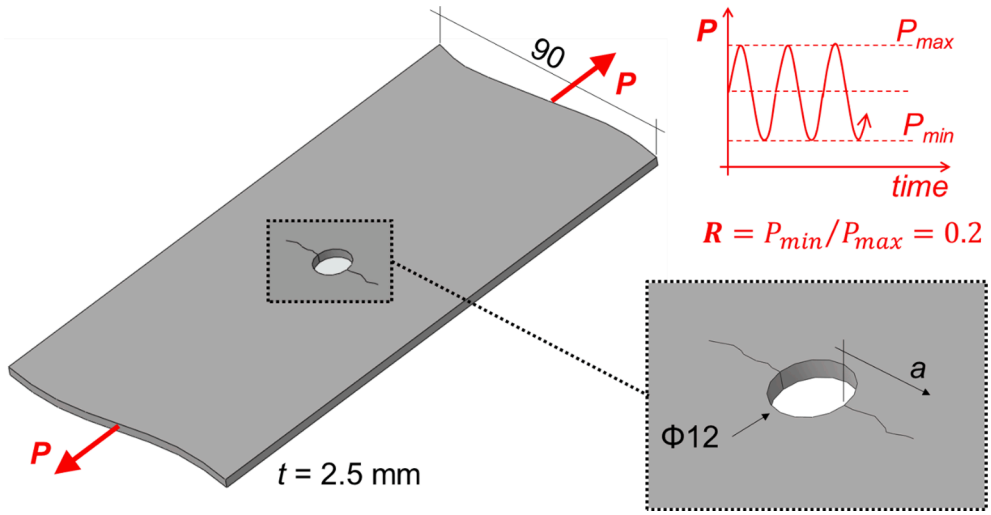

Fig. 2. Case study description: CAD model with highlights of the loading conditions and the central hole from which two cracks can nucleate.

runtimes. Many applications can be found in literature in this regard that demonstrate sound agreements with experimental observations [35], even when only deterministic predictions are considered [25]. However, when the need to deliver a robust (e.g. probabilistic) prediction arises, runtimes of FEM can become unacceptable. Also for Structural Health Monitoring (SHM) applications, the usage of FEM results to be unlikely, even though some procedures have been proposed in literature to circumvent these issues [1,36,37].

Recently, Neural Networks (NNs) have been successfully used to solve engineering issues due to the availability of a great number of datasets gathered from physical experiments or numerical simulations [38–40]. Traditional methods are not able to generalize due to the high variability of the data, whereas NNs can offer more precise assessments under highly variable and uncertain experimental conditions [40]. With the increase in datasets' size and complexity, NNs are able to process information more accurately and complexly. Deep convolutional NNs are often used for two or three-dimensional image and video processing [41,42], but they are also used to extract deep features from one-dimensional data such as speech signals or raw input data vectors for various tasks. Combining traditional computational methods with deep NNs has shown great promise also for fracture analyses [43–48], simulating both the propagation direction and the residual life [49]. Additionally, there is literature on using deep NNs for fatigue life prediction of structures with uncertain parameters, and for real-time monitoring processes [50,51].

This research attempts to fill some of the currently existing literature gaps by combining traditional and shallow/deep learning methodologies for structural life prediction applications. The paper discusses the development of NNs to perform FCG predictions of mechanical structures with high accuracy, in real-time and under uncertain and highly variable input data.

In more detail, FCG simulations were carried out with FEM by considering a single set of deterministic input parameters. The advancing of the crack through the structure was simulated via FEM, allowing to compute the crack advancing direction and the K values at the crack tip along the growth. Once obtained the variation of the K values vs. crack size a, these data were parametrized so to account for stochastically varying input data, viz. allowing to consider large variations of the input data. Consequently, Monte Carlo (MC) simulations were developed on the FEM results so to accelerate the generation of the numerous amount of life predictions, for a given set of input parameters, needed by NN afterwards. The so obtained data were then used to train and validate multiple NNs architectures that were eventually tested against an independent set of input/output data. This research seeks to identify the best NN configuration and optimizer for residual life prediction when the input parameters are subject to significant variations. To do so, different types of NNs (such as Fully Connected and 1-D Convolutional) and multiple layer depths and hidden layers were compared. The performance of each NN architecture was compared in terms of accuracy, computational runtimes and minimum number of samples needed for training, so to determine the ideal architecture with the strongest generalization power. Finally, the best NN was used to calculate a considerable amount of life predictions for various distributions of the input parameters in a negligible runtime.

The overall description of the approach is shown in Fig. 1.

It is worth noting that a priori information about the distribution functions and ranges of variation of the input parameters was not needed, consistently with real-life cases for which this information is generally unknown. Therefore, this approach allows to save times and costs usually needed to make these evaluations through experimental tests on any specific structure. This investigation can be considered as an example case where this approach has been set up, tested and its validity demonstrated. Such an approach was developed by using a simple mechanical component as a case study, i.e. a thin plate with a central hole from which cracks can nucleate [51]. Though the simplicity of this component, with the appropriate adjustments, the same approach can be easily extended to study larger and more complex industrial components in a straightforward manner. Furthermore, as detailed in section 3, the constructed NNs can provide real-time forecasts on cost-effective GPU devices, making it ideal for SHM applications in real-world engineering problems.

The rest of this document is organised as follows:

Section 2 comprises all the details of the presented approach. Firstly, the fatigue crack propagation simulation using FEM is introduced together with the presentation of the case study. The MC simulation procedure is then briefly detailed and, finally, a description of the NN models is given.

Section 3 reports the results of the proposed approach with an extensive discussion of them. Comparisons among MC results and among the NNs results are presented in terms of both accuracy and computational time. Finally, a probabilistic life assessment is made to show an example of application of the presented approach.

The concluding remarks are given in Section 4.

2. Materials and methods

The procedure presented in this research is based on the interaction of FEM, MC method and NNs with the aim of performing residual life

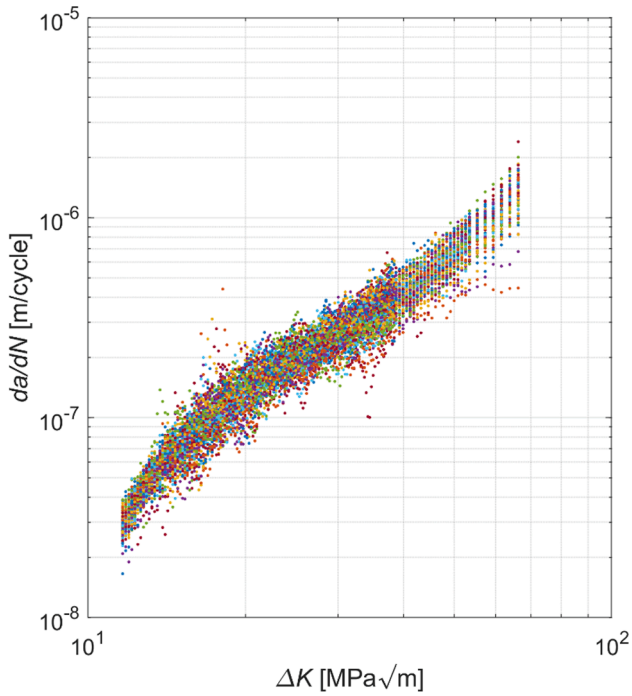

Fig. 3. FCG material data for aluminium alloy 2024-T3. [15,50].

predictions of structures under variable input parameters. The procedure has been presented here as applied to a simple case study, i.e. a thin plate with a central hole under variable and uniaxial loading conditions, see [52–54]. This geometry was chosen thanks to its similarity with the specimens' geometry used to obtain the experimental data adopted in this work [15,55]. Although this application can be considered as an example case only to show the validity of the proposed procedure, this latter can be applied to more complex components by only changing the input FEM model. Hence, no particular complications are expected in extending this procedure to the analysis of a more complex mechanical structure.

All the details of this procedure are provided in this Section.

2.1. Fracture simulation with FEM

The CAD/FEM model of the mechanical component under analysis is shown in Fig. 2. This represents a thin plate with a central hole that can be considered as representative of a bolted joint from which cracks can nucleate at the bolt hole due to the local stress concentration [52–54]. The material of the joint was the aluminium alloy 2024-T3 whose material data related to FCG were available in literature [15,55], see Fig. 3. One crack propagation simulation was carried out on this geometry by assuming two small cracks as triggered at the central hole of the plate, see Fig. 2. The simulation was performed with the commercial code FRANC3D [56] with the main objective of calculating the variation of the K values along the crack-growth as a function of the crack length a. The advancing of the crack was simulated according to geometry, loading conditions and material properties of the plate, by means of a step-by-step incremental procedure (see Fig. 4), thus consisting of the repetitions of the phases of: crack insertion in the model, FEM solving, crack extension and related FEM remeshing. The simulation started by assuming two initial cracks of length $a_0 = 2.0mm$ each and stopped when their lengths were representative of the complete failure of the component ($a_f = 30mm$ each). The initial length of the crack was defined as sufficiently long to justify the usage of a long-crack propagation model. When this cannot be guaranteed, short-crack propagation models or equivalent approaches [27,28] can be considered.

An overall representation of this FEM simulation is reported in Fig. 4. The reader is referred to [1,32,57–59] for further examples and details on how the propagation of cracks can be simulated numerically with FEM.

One of the primary results of a crack-growth simulation is the possibility to predict the residual fatigue life of a mechanical component through the integration of the K vs. a curve with a FCG law calibrated on the experimental data of the material. To this aim, a Paris' law was selected in this work to perform the fatigue cycle counting, see Eqs. (1)–(3):

$$\frac{da}{dN} = C\left[\left(\frac{1-f}{1-R}\right)\Delta K\right]^m \tag{1}$$

$$f = \frac{K_{op}}{K_{max}} = \begin{cases} max\left(R, A_0 + A_1R + A_2R^2 + A_3R^3\right), R \geq 0 \\ A_0 + A_1R, -2 \leq R < 0 \end{cases} \tag{2}$$

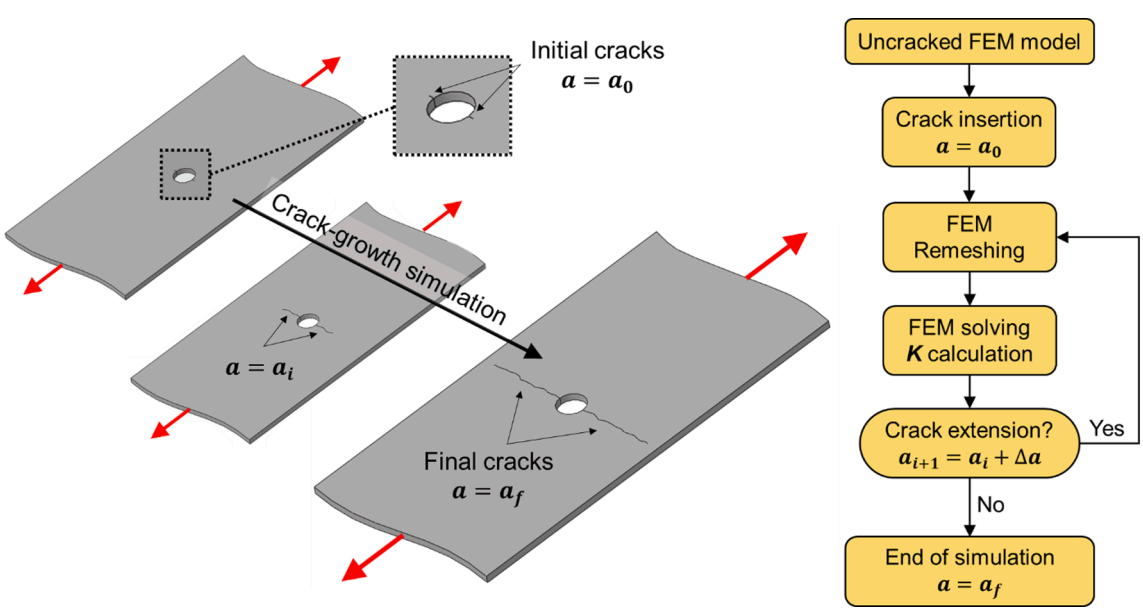

Fig. 4. Description of the incremental FEM simulation of a crack propagation process.

Table 1
Min/Max values for input parameters of MC simulations.

	Distribution	Min value	Max value
Applied load P [kN]	Random	11	17
Initial crack length a_0 [mm]	Random	1.5	2.5
Plate thickness t [mm]	Random	2.1	2.9

$$\left.\begin{aligned} A_0&=(0.825-0.34\alpha+0.05\alpha^2)\left[\cos\left(\frac{\pi}{2}s_{max}/\sigma_0\right)\right]^{1/\alpha}\\ A_1&=(0.415-0.071\alpha)s_{max}/\sigma_0\\ A_2&=1-A_0-A_1-A_3\\ A_3&=2A_0+A_1-1 \end{aligned}\right\} \tag{3}$$

In Eq. (1), N is the number of applied fatigue cycles, a is the crack length, therefore da/dN represents the CGR (i.e. the Crack-Growth Rate), R is the stress ratio equals to $P_{min}/P_{max} = K_{min}/K_{max}$ (set to 0.2 according to the selected experimental tests [15]), whereas ΔK is the stress intensity factor range, equals to $K_{max} - K_{min} = (1-R)K_{max}$. C and m are empirical constants used to modify shift and slope of the CGR curve respectively. As detailed below, C and m do not need to be explicitly defined thanks to the adopted MC procedure. f is the crack opening function that allows to consider a partial contribute of ΔK to the propagation speed da/dN, as reported in [60–62].

In Eq. (3), α is a plane stress/strain constraint factor (set to 1.5), whereas s_{max}/σ_0 ($=0.14$) is the ratio of the maximum applied stress s_{max} to the flow stress σ_0, this latter generally considered as $\sigma_0 = (\sigma_{YS}+\sigma_{UTS})/2$ ($\sigma_{YS} = 381.8MPa$ and $\sigma_{UTS} = 496.2MPa$). As explained in [1,55,57], C and m warrant a modelling as distributions whereas α and s_{max}/σ_0, which do not play a significant role in a life prediction calculation, can be left as constant values.

2.2. Probabilistic fatigue life assessment with MC method

Only one FRANC3D FEM simulation was needed to simulate the crack propagation through the component. This allowed to obtain the variation of the K values as a function of the crack length a and, once obtained the K vs. a curve, this curve was parametrized so to account for stochastically varying input data, thus allowing to consider any possible variation of the input data. These variations were considered through the MC method implemented within MATLAB [63] in such a way to accelerate the generation of the numerous amount of life predictions typically needed to train a NN. A procedure similar to that reported in [52] was adopted in this work for the MC simulations. The reader is referred to [1,55,57,58,64] for further reading, whereas only an overall description is reported herein.

Each MC simulation started with the sampling of the two material parameters C and m so to generate a FCG curve (material data α and s_{max}/σ_0 were kept as constants [1,57]). Such a curve was then compared with the experimental data for a validation and, if judged as acceptably correlating the test data (when $RMS < 2\%$), it was used for a life prediction. This prediction was calculated by using a K vs. a curve computed with randomly sampled parameters for the applied load P, the initial crack length a_0 and the plate thickness t. The related ranges of variability of input parameters for MC simulations were reported in Table 1. It is worth noting that it was not necessary to enforce specific distribution functions (e.g. Gaussian) to the input parameters, being these MC simulations only required to accelerate the data generation to train and validate the NNs. Specific distributions were instead considered afterwards (Section 3.1) so to account for the actual distributions of data during a probabilistic life assessment.

Through this MC-based procedure, it was possible to perform numerous fatigue life predictions accounting for material scattering (through C and m), uncertainty in the actual applied loads (P), uncertainty in the initial crack length (a_0) and geometrical tolerances (through the thickness t).

2.3. Selection and optimization of NN models

Although MC method did not require a significant computing power for this application, it is still unlikely that it will be used for real-time calculations. Therefore, an ablation study was conducted to determine which NN model was able to accurately predict the residual fatigue life with a reduced computational cost. The ablation study aimed to select the best combination of architectures (see Fig. 5) and optimizers (among ADAM, SGD and LM) that would lead to accurate and fast predictions. In this study, the NN models which are often used for regression tasks in engineering research [40,43–51,65,66] were chosen as the basis to construct more complex ones. Furthermore, a hyperparameter optimization over the values of the learning rate for different types of optimizers and the number of neurons/filters per layer was performed.

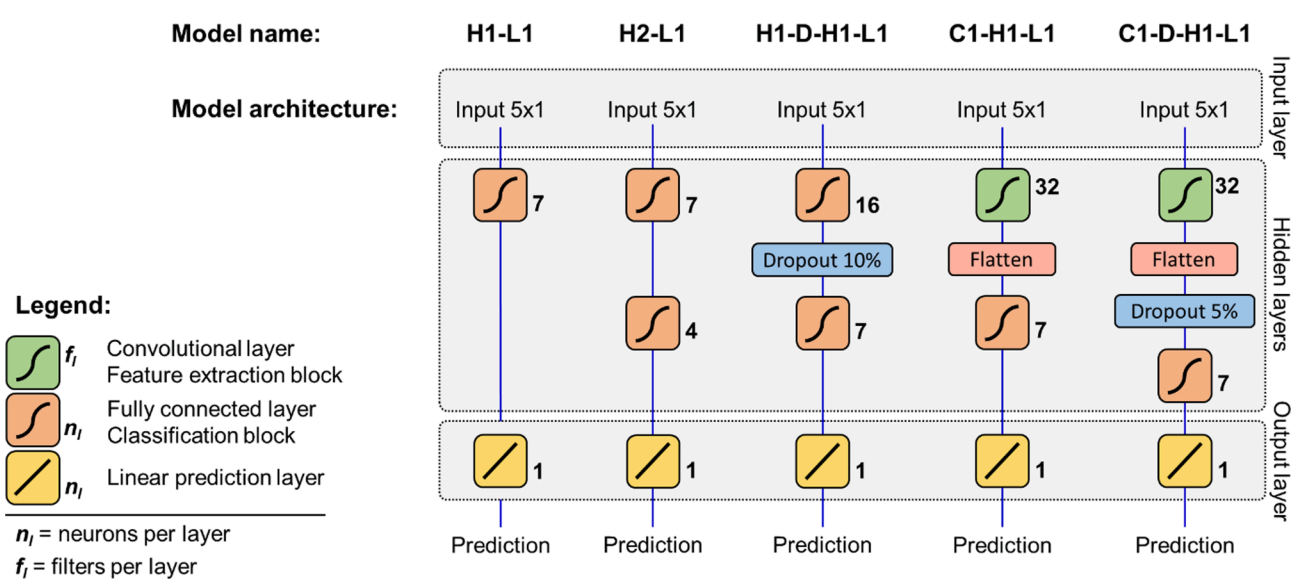

Fig. 5. Scheme of the considered NN architectures. In model names: H symbolizes hidden layers, C stands for 1-dimensional convolutional layers, L represents linear activation layers, dropout layer is indicated by D.

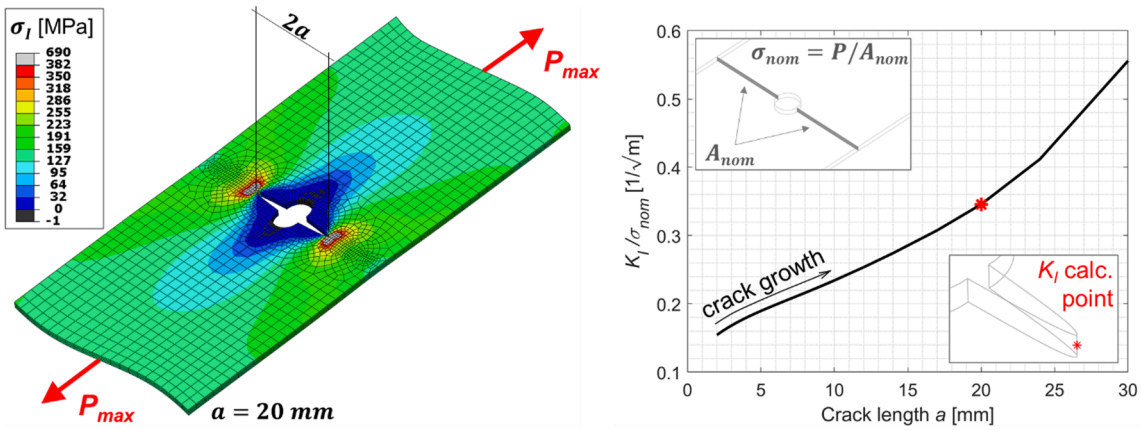

Fig. 6. Maximum principal stress σ_I [MPa] plot at the maximum load P_{max} for an general crack length a of 20 mm; distribution of K_I values along the whole fracture simulation for a unitary nominal stress value σ_{nom}.

Namely, the ablation study aimed to select the best combination of architectures and optimizers keeping as fixed learning rate (set to 0.1 for all models) and number of neurons (see Fig. 5). Once that the two-best performant models were designated, hyperparameter tuning was settled down by changing gradually the learning rate (ranging from 0.0001 to 0.5) and the number of neurons/filters per layer.

To this aim, MC simulations were performed until a total of 10 k combinations of input and output parameters were computed (~5 min of run on a mid-budget laptop). As described in the previous paragraphs, the parameters (C, m, P_{max}, t, a_0) represented the input for the NNs while the target was the residual fatigue life N_f in log scale. All data provided as input and target were normalized in a 0–1 range by considering material data C and m as ranging between (−10.3, −9.1) and (2.3, 3.5) (as obtained in [15,55]), whereas ranges listed in Table 1 were used for P_{max}, t and a_0. The NNs target was constrained into the interval from 4.2 to 5.5 since this was the range of variation for N_f obtained with MC method, see Section 3. Training, validation and test sets remained the same in the ablation study, while different model architectures and optimizers were tested. All NNs were trained using a training set of 8 k records, validated with a validation set of 2 k records, and tested considering two further 10 k records as test sets.

The five NN architectures and the three optimizers compared in the ablation study were mainly characterized by shallow fully connected-dense or hybrid one-dimensional convolutional/dense NNs configured to address a regression task. Fig. 5 shows the first three shallow NNs built with fully connected layers (in orange) and the last two hybrid-architectures comprising convolutional layers (in green). All models were designated by using H for the number of hidden layers, C for the number of 1-D convolutional layers, L for the Linear prediction layer (the last layer in the architecture), D for the dropout. Utilizing non-linearities via the activation function allowed the networks to learn intricate relationships in the data. Thus, before the ablation study, the most well-known activation functions (such as Rectified Linear Unit, Softmax, etc.) were tested to ascertain the most suitable for the current models. Such tests allowed to identify that the sigmoidal activation function was the best choice for H and C layers in all of the presented models.

H1-L1 comprises just one hidden layer and is the simplest model, while H1-D-H1-L1 is slightly more complex and contains two H layers and a dropout layer with a 10% drop rate. The fourth and fifth models, i.e. C1-H1-L1 and C1-D-H1-L1, comprises a 1-D convolutional layer with 32 filters and a kernel size of 2, followed by a flatten layer and a fully connected layer. The fifth model also contains a dropout layer with a 5% drop rate.

The optimizers chosen for this ablation study were: Stochastic Gradient Descent (SGD) [67], ADAM (Adaptive Model Estimation) and Levenberg-Marquardt (LM) (a second-order optimizer) [68]. ADAM is an optimization algorithm that uses past information of the gradient to adapt the learning rates of each parameter, SGD is a simpler optimization algorithm that requires direct tuning of the learning rate, LM is an optimization algorithm well-suited for non-linear least squares problems on datasets with low complexity. At the training step, LM is a combination of SGD and the Newton's method, much faster than the traditional SGD. Meanwhile, SGD updates the parameters of the NN in the direction of the negative gradient of the loss function MSE with respect to the parameters. Finally, ADAM is an optimization algorithm that combines the advantages of both SGD and RMSProp (Root Mean Square Propagation). This adaptive algorithm utilizes the moving averages of parameters in order to compute the second raw moments of the gradients and adjusts the learning rates for each parameter based on the prior gradient data, hence the "adaptive" term in its name.

The Mean Squared Error (MSE; Eq. (4)) metric was utilized as loss function to drive the selected optimizers to minimize the divergence between the predicted value and the true value. Also the Mean Average Error (MAE; Eq. (5)) was considered for monitoring purposes only since less sensitive to outliers than MSE. Coefficient of determination R^2 and MAE were considered for performance monitoring purposes only.

$$MSE = \frac{1}{s}\sum_{1}^{s}\left(N_f^* - N_f\right)^2 \tag{4}$$

$$MAE = \frac{1}{s}\sum_{1}^{s}\left(N_f^* - N_f\right) \tag{5}$$

$$R^2 = 1 - \sum_{1}^{s}\left(N_f - N_f^*\right)^2 / \sum_{1}^{s}\left(N_f - \overline{N_f}\right)^2 \tag{6}$$

where $\overline{N_f}$ represents the average value of N_f.

For each optimizer, the underlying non-linear function inferred by the input data is traced through the propagation of the predictions from the previous layers to the next one, and the weights of the NN models are updated by backpropagating the predictions over the training epochs. It is worth noting that if the learning rate is set too high, it could lead to drastic changes in the optimization, while if too low, the training process could become very slow and imprecise. For all models, in the last fully connected layer L, the optimizers are regularized both at the kernel and at the bias levels by Euclidean norm (L2-norm) [69] based penalty function with the fixed parameter at 0.06. Additionally, bias and kernels of the last layers are initialized using a Glorot Uniform distribution [70] with a fixed seed to potentially reduce overfitting. The convergence of the models was determined by running multiple learning rates and epochs. It was observed that all models achieved convergence prior to the 300th epoch with batch size 1000. The estimators of the models were

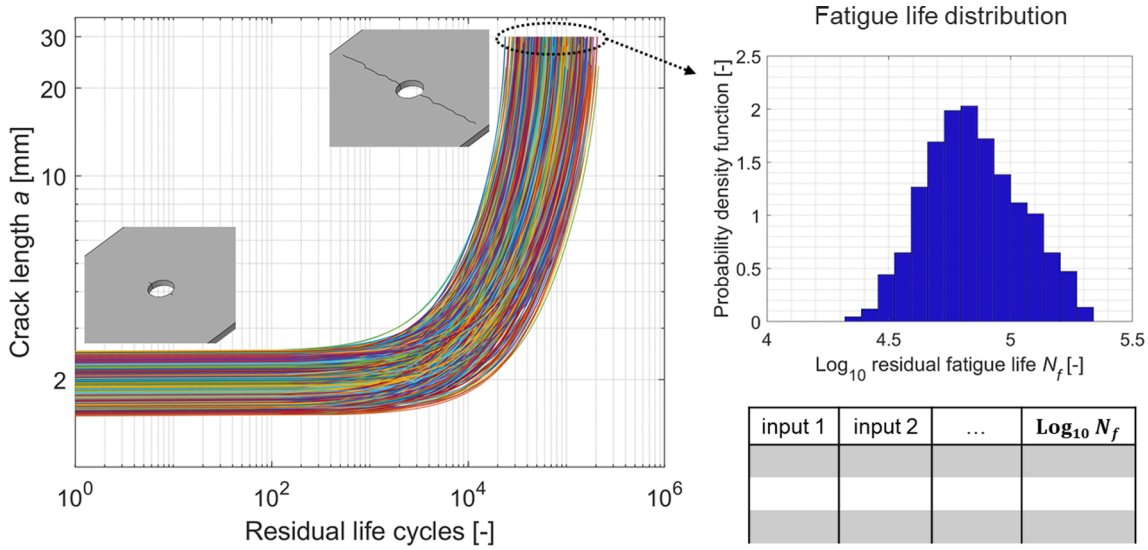

Fig. 7. Probabilistic fatigue life assessment performed with the MC method (input data of Table 1); table reporting an example of data provided to NNs for their training.

determined by the checkpoints obtained at the termination of every training epoch, based on the minimum loss attained on the validation set throughout the training process. The output of the 5 NNs was a prediction of N_f* in the range between 0 and 1. These predictions were then converted back to their original range by using the inverse min–max normalization function.

3. Results and discussion

The presented approach for fatigue life assessment accounted for the uncertainty coming from material scattering, the main geometrical tolerances, loading conditions and the inherent uncertainty in knowing the actual sizes of the defects. The FEM model shown in Fig. 2 was used as a

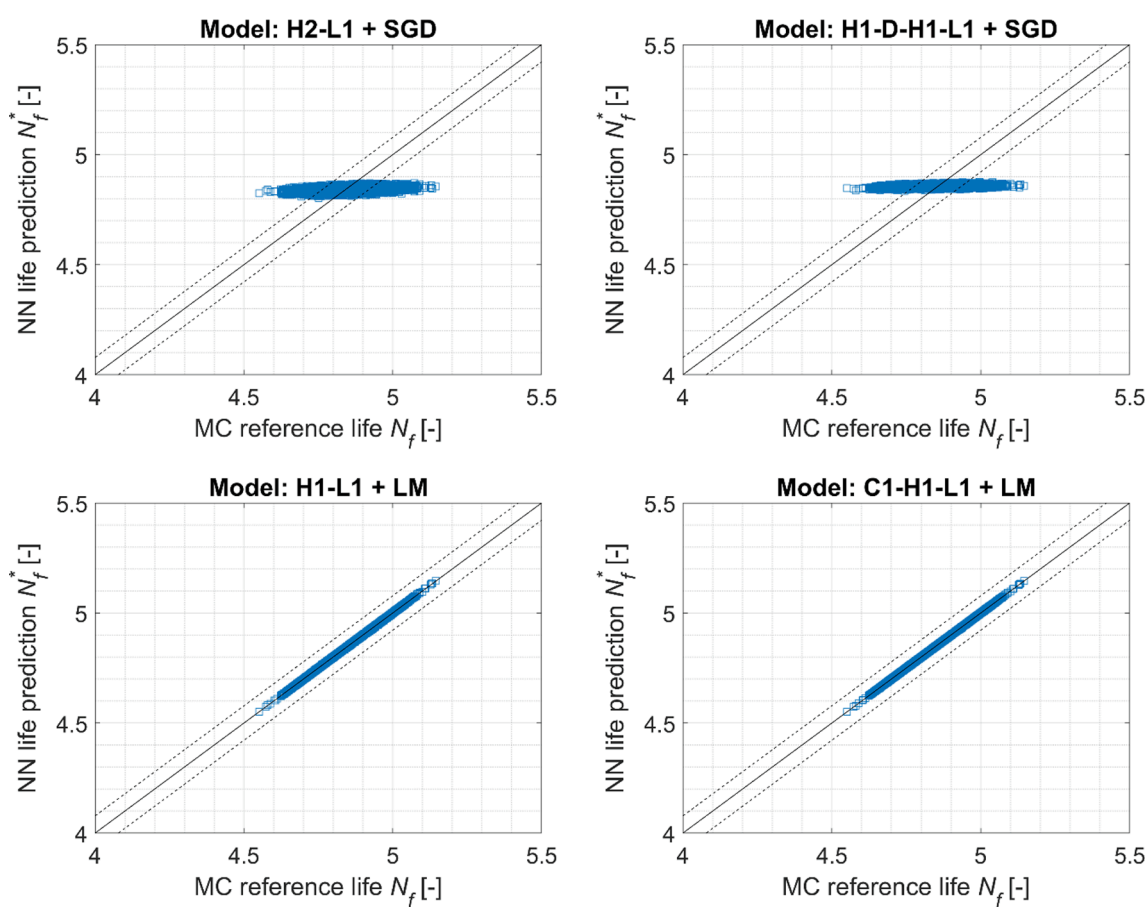

Fig. 8. Comparison of residual fatigue lives obtained with MC method and some NNs configurations; perfect replication observed only when using LM optimizer; all NN configurations not reported for brevity.

Table 2
NNs information and results.

Architecture	Optimizer	MSE	MAE	R^2	Parameters	Runtime [ms]
H1-L1	**LM**	**4.8e-7**	**5.5e-4**	**0.99**	**50**	**22**
H1-L1	SGD	3.7e-3	4.9e-2	0.04	50	17
H1-L1	ADAM	2.7e-3	4.1e-2	0.86	50	18
H2-L1	LM	1.7e-6	1.0e-3	0.93	79	21
H2-L1	SGD	3.8e-3	6.1e-2	0.02	79	18
H2-L1	ADAM	3.3e-3	4.6e-2	3.7e-5	79	18
H1-D-H1-L1	LM	4.2e-4	1.7e-2	0.98	223	27
H1-D-H1-L1	SGD	3.8e-3	4.9e-2	0.02	223	17
H1-D-H1-L1	ADAM	3.2e-3	4.5e-2	1.1e-6	223	18
C1-H1-L1	**LM**	**3.4e-7**	**4.4e-4**	**0.99**	**1007**	**16**
C1-H1-L1	SGD	3.8e-3	4.9e-2	0.05	1007	16
C1-H1-L1	ADAM	2.5e-3	1.3e-2	0.04	1007	17
C1-D-H1-L1	LM	1.2e-4	9.1e-3	1.9e-4	1345	25
C1-D-H1-L1	SGD	3.5e-3	4.7e-2	1.0e-3	1345	20
C1-D-H1-L1	ADAM	3.5e-3	4.7e-2	2.5e-6	1345	17

starting point for a crack propagation simulation. The results obtained with this simulation were reported in Fig. 6 with reference to a general intermediate crack length a of 20 mm. The distribution of K_I values (for a unitary nominal stress value σ_{nom}) in Fig. 7 is that calculated at half thickness, see insets in Fig. 7. Negligible K_{II} and K_{III} were obtained due to the chosen pure Mode-I case study. The reliability of these results was not double checked here even though many other cross-validations have already been documented [1,25,32,59].

Afterwards, MC method was used to perform the life prediction allowing for a probabilistic fatigue life assessment of the cracked component. Such results were summarised in Fig. 7. An average value of 10^4.86 = 72 k fatigue cycles was computed, even though, it is worth noting that the life distribution demonstrated a large range of variability, with the fatigue life ranging between 29 k and 179 k cycles, if assuming a $\mu \pm 3\sigma$ of variation (99.7% of probability).

For sake of clarity, it is worth reiterating that the life distribution shown in Fig. 6 was computed by considering input parameters varying in the ranges reported in Table 1. Therefore, this life distribution has to be considered as an intermediate result only, being arbitrary the distributions of the input data considered for its generation. Nevertheless, the purpose of this intermediate calculation was not the thorough lifespan estimate but only the generation of data to feed the NNs so as to build up mathematical models that allow to perform these quantifications. Indeed, once trained the NNs, more realistic input data distributions were considered and, consequently, a reliable probabilistic life assessment was obtained, see Section 3.1.

As described in Section 2.3, five NN architectures of increasing complexity were implemented, including a shallow NN (which is often used in engineering for regression tasks) and ultimately culminating in a mixed-convolutional NN. A total of 10 k samples was generated with MC as training dataset for the NNs. Five parameters were considered as input to the networks (material data C and m, thickness t, initial crack size a_0, maximum load P_{max}) whereas the only output was the predicted residual fatigue life N_f* in log scale, see Fig. 7.

A comparison of residual fatigue lives obtained with MC method (i.e. the reference data) and those obtained with the trained NNs was

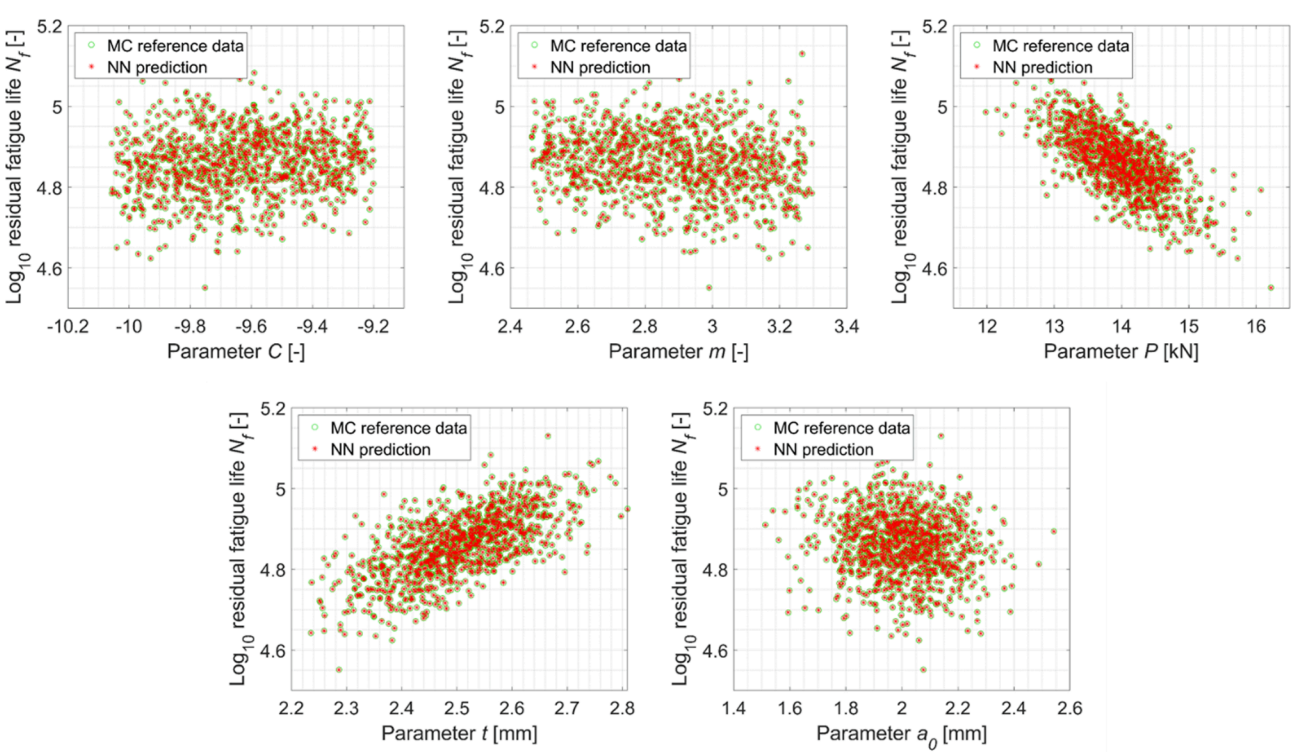

Fig. 9. Scatter plots of input/target relationships for C1-H1-L1 model with LM optimizer on the test dataset; similar good replications observed only for LM optimizer; all configurations not reported for brevity; only 1 k data are shown to improve readability.

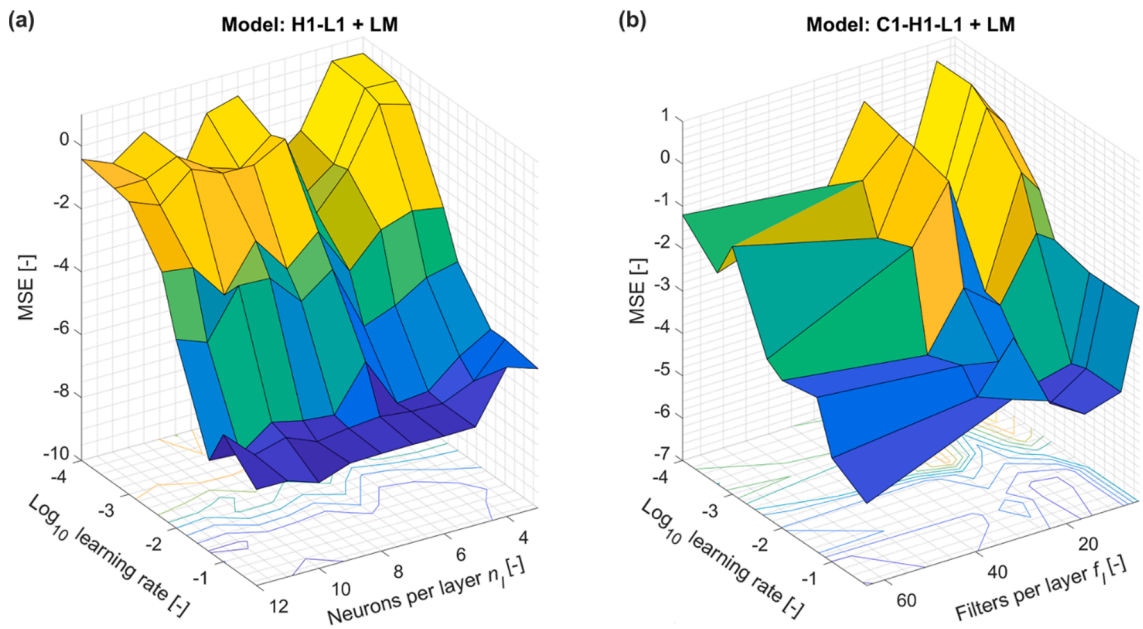

Fig. 10. Results of hyperparameter optimization for NN architectures (a) H1-L1 and (b) C1-H1-L1 (both with LM optimizer).

reported in Fig. 8. A comparison of performances among the NNs was instead reported in Table 2. Despite the relative simplicity of the NNs employed, the ablation study revealed that the three models H1-L1, H2-L1 and C1-H1-L1 yielded impressively low reconstruction errors when driven by the LM optimizer. Effectively, the ablation study clearly demonstrated that the LM optimizer yielded the best results for all configurations and over the same models when driven by SGD and ADAM optimizers. These latter optimizers did not provide sufficient correlation, see Fig. 8. The addition of dropout layers in NN architectures often improves generalization ability, however this was not the case. Indeed, models without dropout were more effective, as the use of a dropout layer led to a decrease in the accuracy of predictions, even when the drop rate was low. The best model in terms of performance was C1-H1-L1 (and LM optimizer), with a reasonable threshold between learnable parameters and prediction time. However, the relatively simplistic nature of the first shallow network H1-L1 (with LM optimizer) resulted to be the second-best model. From the architectural point of view, in the first model, the 1-D convolutional operation, leads to a richer feature abstraction and projection in a more complex feature space, thereby providing more meaningful information to the next fully connected layer. Conversely, in the second model, the presence of a fully-connected layer made it better suited for a robust and non-linear regression task. In both the cases, all the proposed NNs were capable of predicting the desired data with a reasonable accuracy.

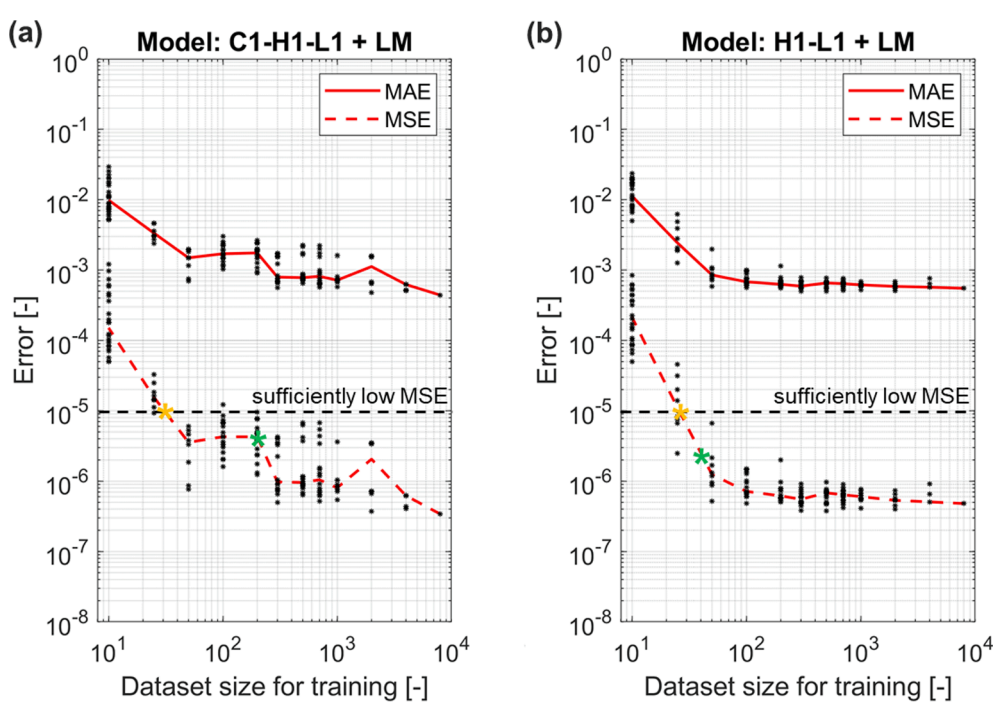

Fig. 11. NN prediction errors for tests as a function of the dataset size used for NN training: (a) C1-H1-L1 and (b) H1-L1 architectures (both with LM optimizer); yellow and green asterisks stand for the dataset sizes returning well-trained NNs with 50% and 100% of probability respectively.

A perfect replications of MC results with the trained NNs was evident for mostly all NN architectures optimized with LM. Same conclusions can be draw by also looking at the scatter plots reported in Fig. 9 where it can be noticed that all trends were correctly captured by NNs trained with the LM optimizer. Besides the perfect replication of data achieved through the NNs, a comparison was also arranged (Table 2) in terms of computational runtimes, especially relevant when the NN has to be implemented in a small GPU device, like NVIDIA Jetson Nano, for SHM.

A hyperparameter optimization over the values of the learning rate for different types of optimizers and the number of neurons/filters was performed. Results of such optimization were reported in Fig. 10 by considering MSE as key parameter performance. Namely, the ablation study aimed to select the best combination of architectures and optimizers maintaining the learning rate fixed to 0.1 and the number of neurons/filters fixed to those reported in Fig. 5. Then, once the two-best performant models were selected (see e.g. Table 2), hyperparameter tuning was settled down by gradually changing learning rate and number of neurons/filters. All relevant parameters and hyperparameters out from the hyperparameter optimization were kept in a fixed configuration to ensure fairness, e.g. batch size, error regularizers, as well as all the seeds used to control models' randomness (e.g. Bias and Kernel initializers, dropout pruning strategy, etc.).

Fig. 10 displays how the MSE changes for the two best models by varying these two hyperparameters. Regarding the H1-L1 model (Fig. 10a), the best learning rate resulted to be around 0.1 ÷ 0.5, thus validating the previously considered value of this hyperparameter. On the other hand, no particular variation was observed by increasing/decreasing the number of neurons. Regarding the C1-H1-L1 model (Fig. 10b), both hyperparameters resulted to play a role, with the lowest MSE given by the highest learning rate and the highest number of filters, perhaps suggesting that bigger values would deliver even better performances. However, the downside is that increasing these parameters would produce longer runtimes, to not count the fact that these MSEs are much higher than those provide by H1-L1 in any case.

It is evident that all NNs, especially C1-H1-L1 and H1-L1 models with LM optimizer, demonstrated very good accuracy when 8 k input/output data are considered as training dataset size. Although 8 k data can be easily calculated through the adopted FEM-MC procedure, it could be of interest to evaluate the minimum dataset size that allows to reach an acceptable accuracy. To this aim, C1-H1-L1 and H1-L1 models were repeatedly trained with reduced amount of data randomly sampled among the 10 k already available. This to determine how many records were necessary before the network's generalization power on the problem decreased. It is important to emphasize that, for each sample size, the training set was randomly selected without repetition proportionally to its size; for example, with a training set comprising 8 k records with a sample size of 1 k, only 8 non-overlapping samples of 1 k records were used for individual retraining.

The so obtained prediction errors (MSE and MAE) were reported with black dots in Fig. 11 as a function of the dataset size used for training (red lines represent the median values). As expectable, the larger the training dataset size, the lower the prediction errors. Best model resulted to be H1-L1 providing better performances than C1-H1-L1 when considering reduced amount of training data. This because H1-L1 presents a smaller number of trainable parameters with respect to C1-H1-L1. H1-L1 demonstrated decreasing dispersions of prediction errors by increasing the dataset size, consistently with the expectations. This was not the case of C1-H1-L1 model, suggesting that the lowest error obtained with 8 k training data could have been just a lucky outcome.

By visual observation of the so obtained life predictions, it can be roughly defined that a MSE of 1e-5 can be considered as a sufficiently low error value. Therefore, with reference to the H1-L1 model, it resulted that nearly 25 data are needed to guarantee 50% of probability of achieving a well-trained NN (yellow asterisk in Fig. 11b), whereas 30 to 40 data are instead needed for a probability around 100% (green asterisk in Fig. 11b). Similarly, C1-H1-L1 requires nearly 30 data for a 50% of probability, whereas an enormously larger dataset (1 k to 2 k data) seems to be required to guarantee sufficiently low MSE errors. These results give indications on the number of simulations and/or experimental data needed to set up a life prediction model based on NNs (with LM as optimizer). If considering also that these data are randomly generated, a proper set up of the Design of Experiment would also reduce the here defined data requirements.

Table 3
Min/Max values of input parameters for the probabilistic life assessment.

Contributor	Distribution	Mean value	Standard deviation
Maximum applied load P_{max} [kN]	Gaussian	14	0.7
Initial crack length a_0 [mm]	Gaussian	2.0	0.17
Plate thickness t [mm]	Gaussian	2.5	0.1
Material scattering [-]	quantified based on material data of Fig. 2.		

3.1. Probabilistic life assessment

Many factors can influence the residual life of a structure, such as geometrical factors, material variability, statistical uncertainty, uncertain loading conditions, modelling approximations, etc. All these contributors can have an effect that either cannot be reduced in size but needs to be quantified or cannot be estimated at all because of lack of information. Probabilistic lifing methodologies attempt to fill some of these gaps through more robust predictions than those provided by deterministic tools allowing to avoid unnecessary conservativism.

In this work, the fatigue life prediction models developed by means of NNs were designed in order to be able to output probabilistic life distributions in real-time. Material scattering, loading conditions, initial crack size and geometrical tolerances were considered here as being the principal sources of uncertainty appearing during this structural integrity assessment. A realistic probabilistic life assessment was performed with the best NN (i.e. H1-L1) by considering the ranges of variation provided in Table 3. Namely, if considering a $\mu \pm 3\sigma$ of variation (99.73% of probability), the maximum applied load P_{max} was considered as varying in the range 14 ± 2.0 kN, the thickness of the plate t in the range 2.5 ± 0.3 mm, the initial crack size a_0 in the range 2.0 ± 0.5 mm. The adoption of Gaussian distributions for geometrical tolerances and loading conditions can be considered as a common engineering practice for many engineering problems [16,17,57,58,71,72]. Although more debatable, also the initial crack size a_0 was considered as following a Gaussian distribution, as similarly assumed in [59]. Instead, material scattering was quantified through the MC procedure presented in Section 2, therefore no specific distributions were arbitrarily enforced.

It is worth noting that the NNs were trained by considering the potential variation of input data and, therefore, they can be used to deliver fatigue life predictions as a distribution. At the same time, in-situ measurements for SHM are generally made through accelerometers, strain gauges and/or load cells, hence they are usually deterministic data (with known measurement errors). Therefore, the so trained NNs can be used to calculate deterministic life predictions, when fed by deterministic data, or can produce probabilistic life distributions, when fed by distributions of data. Additionally, measurements accuracies are generally contributes known a priori and, therefore, probabilistic life distributions can be estimated even when only (deterministic) sensor measurements are available in real-time if coupling these measurements with their known ranges of variation. Same holds true for material scattering and geometrical tolerances that represent two contributes whose variations can be quantified off-line.

The results of the probabilistic life assessment were reported in Fig. 12. The overall fatigue life distribution can be well replicated by a lognormal distribution with an average value of 10^4.86 = 72 k fatigue cycles. Although more realistic Gaussian distributions were considered

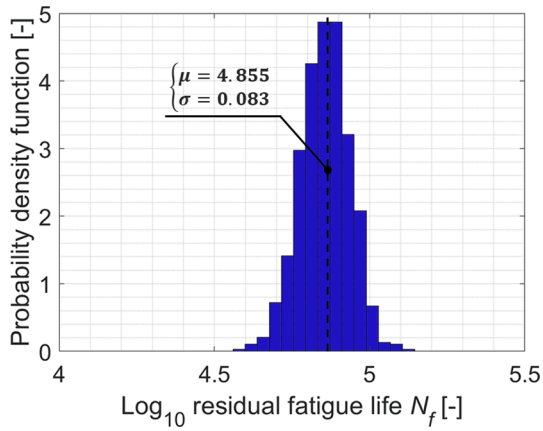

Fig. 12. Probabilistic fatigue life assessment performed with the NN model H1-L1 (input data of Table 3); MC reference data are completely overlapped.

(instead of those random as per Fig. 7 results), this distribution demonstrated a large range of variability, with the fatigue life ranging between 40 k and 127 k cycles, if assuming a $\mu \pm 3\sigma$ of variation (99.7% of probability). This range of variability of the component life came from unavoidable sources of uncertainty, such as the inherent scattering of material data and initial crack size uncertainty, as well as from more controllable parameters, such as the geometrical tolerances and the loading conditions. Quantifying and controlling all these parameters during the in-service life of mechanical components is essential to quantify the probability of failure so as to guarantee safety [57,59].

4. Conclusions

This research presented an innovative methodology that allows to construct models able to perform probabilistic residual life predictions in real-time and under uncertain input data.

Such a methodology was developed through a collaboration of advanced FEM crack-growth simulations, MC method and complex multi-level NNs. FEM was used to simulate the propagation of a crack by considering a simple mechanical structure (i.e. a thin plate with a central hole) as a demonstrator for the proposed methodology. Consequently, MC method was used to generate the output data (residual fatigue lives) needed as input for training the NNs. Particularly, five different NNs architectures and 3 different optimizers were set up and benchmarked so to determine the ideal model architecture.

Results demonstrated that the most part of the considered NNs perfectly replicated the MC reference data, in particular those adopting the LM optimizer. The mixed model, which included 1-d convolutional and fully-connected layers, had the best level of accuracy (with a MSE of 3.4e-7 on the test set) when trained with a large number of records. Nonetheless, the shallow model (H1-L1) resulted to be the best choice since demonstrating a comparable accuracy (MSE of 4.8e-7 on the test set) and much better and stable results for lower amount of data. Additionally, since requiring only very few parameters, its potential applicability for SHM purposes in small cost-effective GPU devices resulted to be more attractive.

Finally, the best model (H1-L1) was used to perform a probabilistic fatigue life assessment as a demonstrator for its potential applicability for real case scenarios where uncertainty of data and measurements is typical.

Declaration of Competing Interest

The authors declare that they have no known competing financial interests or personal relationships that could have appeared to influence the work reported in this paper.

Data availability

Data will be made available on request.

References

[1] Giannella V. Stochastic approach to fatigue crack-growth simulation for a railway axle under input data variability. Int J Fatigue 2021;144:106044. https://doi.org/10.1016/j.ijfatigue.2020.106044.
[2] Sepe R, Greco A, De Luca A, Armentani E, Berto F. Experimental and FEM numerical assessment of multiaxial fatigue failure criteria for a rolling Stock's seats structure. Eng Fail Anal 2019;102:303–17. https://doi.org/10.1016/j.engfailanal.2019.04.065.
[3] S. Romano, S. Beretta, S. Miccoli, M. Gschweitl. Probabilistic Framework for Defect Tolerant Fatigue Assessment of Additively Manufactured Parts Applied to a Space Component, in Structural Integrity of Additive Manufactured Parts. In: Shamsaei N, Daniewicz S, Hrabe N, Beretta S, Waller J, Seifi M, editors, West Conshohocken, PA: ASTM International, 2020), 526-539. 10.1520/STP162020180112.
[4] Citarella R, Giannella V, Vivo E, Mazzeo M. FEM-DBEM approach for crack propagation in a low pressure aeroengine turbine vane segment. Theor Appl Fract Mech 2016;86:143–52.
[5] Giannella V, Fellinger J, Perrella M, Citarella R. Fatigue life assessment in lateral support element of a magnet for nuclear fusion experiment "Wendelstein 7-X". Eng Fract Mech 2017;178:243–57. https://doi.org/10.1016/j.engfracmech.2017.04.033.
[6] Fellinger J, Citarella R, Giannella V, Lepore M, Sepe R, Czerwinski M, et al. the W7-X team. Overview of fatigue life assessment of baffles in Wendelstein 7-X. Fusion Eng Des 2018;136(A):292–7. https://doi.org/10.1016/j.fusengdes.2018.02.011.
[7] Carlone P, Citarella R, Sonne MR, Hattel JH. Multiple crack growth prediction in AA2024-T3 friction stir welded joints, including manufacturing effects. Int J Fatigue 2016;90:69–77. https://doi.org/10.1016/j.ijfatigue.2016.04.004.
[8] Rubino F, Canale G, Sathujoda P. The effect of manufacturing defects on the high-cycle fatigue of electron-beam-welded Ti-6Al-4V titanium alloy: experimental and numerical analysis. Multidiscip Model Mater Struct 2021;17(4):796–813. https://doi.org/10.1108/MMMS-09-2020-0230.
[9] Rubino F, Parmar H, Esperto V, Carlone P. Ultrasonic welding of magnesium alloys: a review. Mater Manuf Process 2020;35(10):1051–68. https://doi.org/10.1080/10426914.2020.1758330.
[10] Vedernikov A, Tucci F, Carlone P, Gusev S, Konev S, Firsov D, et al. Effects of pulling speed on structural performance of L-shaped pultruded profiles. Compos Struct 2021;255:112967. https://doi.org/10.1016/j.compstruct.2020.112967.
[11] Caggiano A, Zhang J, Alfieri V, Caiazzo F, Gao R, Teti R. Machine learning-based image processing for on-line defect recognition in additive manufacturing. CIRP Ann 2019;68(1):451–4. https://doi.org/10.1016/j.cirp.2019.03.021.
[12] Caggiano A, Teti R, Alfieri V, Caiazzo F. Automated laser polishing for surface finish enhancement of additive manufactured components for the automotive industry. Prod Eng 2021;15(1):109117. https://doi.org/10.1007/s11740-020-01007-1.
[13] Sahadi JV, Nowell D, Paynter RJH. Fatigue life prediction for waspaloy under biaxial loading. Theor Appl Fract Mech 2018;97:1–14.
[14] Beber VC, Schneider B, Brede M. Efficient critical distance approach to predict the fatigue lifetime of structural adhesive joints. Eng Fract Mech 2019;214:365–77.
[15] Virkler DA, Hillberry BM, Goel PK. The statistical nature of fatigue crack propagation ASME. J Eng Mater Technol 1979;101(2):148–53.
[16] Beretta S, Foletti S, Rusconi E, Riva A, Socie D. A log-normal format for failure probability under LCF: concept, validation and definition of design curve. Int J Fatigue 2016;82:2–11. https://doi.org/10.1016/j.ijfatigue.2015.08.027.
[17] Citarella R, Apicella A. Advanced design concepts and maintenance by integrated risk evaluation for aerostructures. SDHM Struct Durability Health Monitor 2006;2(3):183–96. https://doi.org/10.3970/sdhm.2006.002.183.
[18] Sandberg D, Mansour R, Olsson M. Fatigue probability assessment including aleatory and epistemic uncertainty with application to gas turbine compressor blades. Int J Fatigue 2017;95:132–42. https://doi.org/10.1016/j.ijfatigue.2016.10.001.
[19] Endeshaw HB, Ekwaro-Osire S, Alemayehu FM, Dias JP. Evaluation of fatigue crack propagation of gears considering uncertainties in loading and material properties. Sustainability 2017;9(12):2200. https://doi.org/10.3390/su9122200.
[20] Peng X, Atroshchenko E, Atroshchenko E, Kerfriden P, Bordas SPA. Isogeometric boundary element methods for three dimensional static fracture and fatigue crack growth. Comput Methods Appl Mech Eng 2017;316:151–85.
[21] Dell'Erba DN, Aliabadi MH. DBEM analysis of fracture problems in three dimensional thermoelasticity using J-integral. Int J Solids Struct 2001;38(26–27):4609–30.
[22] Dhondt G. Automatic 3-D mode I crack propagation calculations with finite elements. Int J Numer Meth Eng 1998;41(4):739–57. https://doi.org/10.1002/(SICI)1097-0207(19980228)41:4<739::AID-NME309>3.0.CO;2-M.
[23] Pan E, Amadei B. Fracture mechanics analysis of cracked 2-d anisotropic media with a new formulation of the boundary element method. Int J Fract 1996;77:161–74.
[24] Pan E. A general boundary element analysis of 2-D linear elastic fracture mechanics. Int J Fract 1997;88:41–59.
[25] Giannella V, Perrella M. Multi-axial fatigue numerical crack propagations in cruciform specimens. Frattura ed Integrita Strutturale 2019;13(48):639–47. https://doi.org/10.3221/IGF-ESIS.48.61.

[26] Giannella V, Dhondt G, Kontermann C, Citarella R. Combined static-cyclic multi-axial crack propagation in cruciform specimens. Int J Fatigue 2019;123:296–307. https://doi.org/10.1016/j.ijfatigue.2019.02.029.

[27] Morse L, Khodaei ZS, Aliabadi MH. A multi-fidelity modelling approach to the statistical inference of the equivalent initial flaw size distribution for multiple-site damage. Int J Fatigue 2019;120:329–41. https://doi.org/10.1016/j.ijfatigue.2018.11.010.

[28] Morse L, Khodaei ZS, Aliabadi MH. Statistical inference of the equivalent initial flaw size for assembled plate structures with the dual boundary element method. Eng Fract Mech 2020;238:107271. https://doi.org/10.1016/j.engfracmech.2020.107271.

[29] Cai YC, Sun P, Zhu HH, Rabczuk T. A mixed cover meshless method for elasticity and fracture problems. Theor Appl Fract Mech 2018;95:73–103.

[30] Zhu HH, Sun P, Cai YC. Independent cover meshless method for the simulation of multiple crack growth with arbitrary incremental steps and directions. Eng Anal Bound Elem 2017;83:242–55.

[31] Pokorný P, Hutař P, Náhlík L. Residual fatigue lifetime estimation of railway axles for various loading spectra. Theor Appl Fract Mech 2016;82:25–32. https://doi.org/10.1016/j.tafmec.2015.06.007.

[32] Citarella R, Giannella V, Lepore M, Dhondt G. Dual boundary element method and finite element method for mixed-mode crack propagation simulations in a cracked hollow shaft. Fatigue Fract Eng Mater Struct 2018;41(1):84–98. https://doi.org/10.1111/ffe.12655.

[33] Beretta S, Carboni M, Regazzi D. Load interaction effects in propagation lifetime and inspections of railway axles. Int J Fatigue 2016;91(2):423–33. https://doi.org/10.1016/j.ijfatigue.2016.03.009.

[34] Amato D, Mayrhofer L, Robl C, Dhondt G, Citarella R. Prediction of the crack growth propagation direction in non-proportional mixed-mode missions. Int J Fatigue 2023;166:107233. https://doi.org/10.1016/j.ijfatigue.2022.107233.

[35] Citarella R, Perrella M. Multiple surface crack propagation: Numerical simulations and experimental tests. Fatigue Fract Eng Mater Struct 2005;28(1–2):135–48. https://doi.org/10.1111/j.1460-2695.2004.00842.x.

[36] Perfetto D, De Luca A, Perfetto M, Lamanna G, Caputo F. Damage detection in flat panels by guided waves based artificial neural network trained through finite element method. Materials 2021;14:7602. https://doi.org/10.3390/ma14247602.

[37] De Luca A, Perfetto D, De Fenza A, Petrone G, Caputo F. Guided wave SHM system for damage detection in complex composite structure. Theor Appl Fract Mech 2020;105:102408.

[38] Zhang JP, Gao PF, Fang F. An ATPSO-BP neural network modeling and its application in mechanical property prediction. Comput Mater Sci 2019;163:262–6.

[39] Rumelhart DE, Hinton GE, Williams RJ. Learning representations by back-propagating errors. Nature 1986;323(6088):533.

[40] Ghiasi B, Jodeiri A, Andik B. Using a deep convolutional network to predict the longitudinal dispersion coefficient. J Contam Hydrol 2021;240:103798. https://doi.org/10.1016/j.jconhyd.2021.103798.

[41] Jodeiri A, Otake Y, Zoroofi RA, Hiasa Y, Takao M, Uemura K, et al. Estimation of pelvic sagital inclanation from anteroposterior radiograph using convolutional neural networks: proof-of-concept study. EPiC Ser Health Sci 2018;2:114–8.

[42] Jodeiri A, Zoroofi RA, Hiasa Y, Takao M, Sugano N, Sato Y, et al., 2019. Region-based Convolution Neural Network Approach for Accurate Segmentation of Pelvic Radiograph. arXiv preprint. arXiv:1910.13231.

[43] Cheng ZX, Wang H. How to control the crack to propagate along the specified path feasibly. Comput Method Appl Mech 2018;336:554–77.

[44] Sbarufatti C, Corbetta M, Manes A, Giglio M. Sequential Monte-Carlo sampling based on a committee of artificial neural networks for posterior state estimation and remaining life time prediction. Int J Fatigue 2015;83(1):10–23. https://doi.org/10.1016/j.ijfatigue.2015.05.017.

[45] Ma X, He X, Tu ZC. Prediction of fatigue–crack growth with neural network-based increment learning scheme. Eng Fract Mech 2021;241:107402. https://doi.org/10.1016/j.engfracmech.2020.107402.

[46] Do DT, Lee J, Nguyen-Xuan H. Fast evaluation of crack growth path using time series forecasting. Eng Fracture Mech 2019;218:106567. https://doi.org/10.1016/j.engfracmech.2019.106567.

[47] Nguyen DLH, Do DTT, Lee J, Rabczuk T, Nguyen-Xuan H. Forecasting damage mechanics by deep learning. Computers Mater Continua 2019;61(3):951–77. https://doi.org/10.32604/cmc.2019.08001.

[48] Bin Younis H, Kamal K, Sheikh MF, Hamza A. Prediction of fatigue crack growth rate in aircraft aluminum alloys using optimized neural networks. Theor Appl Fract Mech 2022;117. https://doi.org/10.1016/j.tafmec.2021.103196.

[49] Baptista R, Moita P, Infante V. Fatigue crack growth on modified CT specimens using artificial neural networks. Int J Fatigue 2022;25:107357. https://doi.org/10.1016/j.ijfatigue.2022.107357.

[50] Feng S, Han X, Ma Z, Królczyk G, Li Z. Data-driven algorithm for real-time fatigue life prediction of structures with stochastic parameters. Comput Method Appl M 2020;372:113373. https://doi.org/10.1016/j.cma.2020.113373.

[51] Wang M, Feng S, Incecik A, Królczyk G, Li Z. Structural fatigue life prediction considering model uncertainties through a novel digital twin-driven approach. Comput Methods Appl Mech Eng 2022;391:114512. https://doi.org/10.1016/j.cma.2021.114512.

[52] Armentani E, Greco A, De Luca A, Sepe R. Probabilistic analysis of fatigue behavior of single lap riveted joints. Appl Sci 2020;10:3379. https://doi.org/10.3390/app10103379.

[53] Armentani E, Laiso M, Caputo F, Sepe R. Numerical FEM evaluation for the structural behaviour of a hybrid (bonded/bolted) single-lap composite joint. Struct Integrity 2018;8:137–53. https://doi.org/10.1016/j.prostr.2017.12.015.

[54] Greco A, De Luca A, Lamanna G, Sepe R. Numerical investigation on the influence of tightening in bolted joints. Procedia Struct Integrity 2019;24:746–57. https://doi.org/10.1016/j.prostr.2020.02.066.

[55] Giannella V. On the statistical nature of fatigue crack-growth through Monte Carlo simulations and experimental data. IOP Conf Ser: Mater Sci Eng 2022;1214. https://doi.org/10.1088/1757-899X/1214/1/012020.

[56] FRANC3D. Reference manual v8. Fracture Analysis Consultants Inc.; 2022.

[57] Giannella V. Uncertainty quantification in fatigue crack-growth predictions. Int J Fract 2022;235:179–95. https://doi.org/10.1007/s10704-022-00624-4.

[58] Giannella V, Sepe R, Citarella R. Fatigue crack propagation for an aircraft compressor under input data variability. Procedia Struct Integrity 2022;41(C):298–304. https://doi.org/10.1016/j.prostr.2022.05.035.

[59] Giannella V, Sepe R, Borrelli A, De Michele G, Armentani E. Numerical investigation on the fracture failure of a railway axle. Eng Fail Anal 2021;129:105680. https://doi.org/10.1016/j.engfailanal.2021.105680.

[60] Newman JC. A Crack Opening Stress Equation for Fatigue Crack Growth. Int J Fract 1984;24:R131–5. https://doi.org/10.1007/BF00020751.

[61] Elber W. Fatigue crack closure under cyclic tension. Eng Fract Mech 1970;2:37–45. https://doi.org/10.1016/0013-7944(70)90028-7.

[62] W. Elber, The Significance of Fatigue Crack Closure, in: Damage Tolerance in Aircraft Structures. In: M. Rosenfeld, editor, West Conshohocken, PA: ASTM International; 1971. p. 230-42. 10.1520/STP26680S.

[63] MATLAB R2020a. Natick, Massachusetts: The MathWorks Inc. 2019.

[64] Giannella V. Fatigue crack-growth predictions for a railway axle under material data variability. IOP Conf Ser: Mater Sci Eng 2021;1038. https://doi.org/10.1088/1757-899X/1038/1/012062.

[65] Agliata A, Giordano D, Bardozzo F, Bottiglieri S, Facchiano A, Tagliaferri R. Machine Learning as a Support for the Diagnosis of Type 2 Diabetes. Int. J. Mol. Sci. 2023;24:6775.

[66] Zuluaga FHG, Bardozzo F, Patino JIR, Tagliaferri R. In: November). Blind microscopy image denoising with a deep residual and multiscale encoder/decoder network. IEEE; 2021. p. 3483–6.

[67] Dogo, E. M., et al. A comparative analysis of gradient descent-based optimization algorithms on convolutional neural networks. In: 2018 international conference on computational techniques, electronics and mechanical systems (CTEMS). IEEE, 2018. 10.1109/CTEMS.2018.8769211.

[68] Sayed A, Sardeshmukh M, Limkar S. Optimisation Using Levenberg-Marquardt Algorithm of Neural Networks for Iris. In: Satapathy S, Udgata S, Biswal B, editors. Proceedings of the International Conference on Frontiers of Intelligent Computing: Theory and Applications (FICTA) 2013. Advances in Intelligent Systems and Computing; 2014, vol. 247. Springer, Cham. 10.1007/978-3-319-02931-3_12.

[69] Girosi F, Jones M, Poggio T. Regularization theory and neural networks architectures. Neural Comput 1995;7(2):219–69. https://doi.org/10.1162/neco.1995.7.2.219.

[70] Glorot X, Yoshua B. Understanding the difficulty of training deep feedforward neural networks. In: Proceedings of the thirteenth international conference on artificial intelligence and statistics. JMLR Workshop and Conference Proceedings, 2010.

[71] Zhu SP, Foletti S, Beretta S. Probabilistic framework for multiaxial LCF assessment under material variability. Int J Fatigue 2017;103:371–85. https://doi.org/10.1016/j.ijfatigue.2017.06.019.

[72] Guida M, Penta F. A Bayesian analysis of fatigue data. Struct Saf 2010;32(1):64–76. https://doi.org/10.1016/j.strusafe.2009.08.001.